Journal of Quantitative Spectroscopy & Radiative Transfer 209 (2018) 137–149

Contents lists available at ScienceDirect

Journal of Quantitative Spectroscopy & Radiative Transfer

journal homepage: www.elsevier.com/locate/jqsrt

# Spatial Heterodyne Observations of Water (SHOW) vapour in the upper troposphere and lower stratosphere from a high altitude aircraft: Modelling and sensitivity analysis

J.A. Langille*, D. Letros, D. Zawada, A. Bourassa, D. Degenstein, B Solheim

*University of Saskatchewan, 116 Science Place - Room 260, Saskatoon, Saskatchewan S7N 5E2, Canada*

ARTICLE INFO

*Article history:*
Received 30 November 2017
Revised 18 January 2018
Accepted 19 January 2018
Available online 31 January 2018

*Keywords:*
Remote sensing
Water vapour
Radiative transfer

ABSTRACT

A spatial heterodyne spectrometer (SHS) has been developed to measure the vertical distribution of water vapour in the upper troposphere and the lower stratosphere with a high vertical resolution (~500 m). The Spatial Heterodyne Observations of Water (SHOW) instrument combines an imaging system with a monolithic field-widened SHS to observe limb scattered sunlight in a vibrational band of water (1363 nm–1366 nm). The instrument has been optimized for observations from NASA's ER-2 aircraft as a proof-of-concept for a future low earth orbit satellite deployment. A robust model has been developed to simulate SHOW ER-2 limb measurements and retrievals. This paper presents the simulation of the SHOW ER-2 limb measurements along a hypothetical flight track and examines the sensitivity of the measurement and retrieval approach. Water vapour fields from an Environment and Climate Change Canada forecast model are used to represent realistic spatial variability along the flight path. High spectral resolution limb scattered radiances are simulated using the SASKTRAN radiative transfer model. It is shown that the SHOW instrument onboard the ER-2 is capable of resolving the water vapour variability in the UTLS from approximately 12 km – 18 km with ±1 ppm accuracy. Vertical resolutions between 500 m and 1 km are feasible. The along track sampling capability of the instrument is also discussed.

© 2018 Elsevier Ltd. All rights reserved.

## 1. Introduction

It is widely accepted that the distribution of water vapour in the Upper Troposphere and Lower Stratosphere (UTLS) region is strongly linked to climate related processes [1–3]. Indeed, the chemical and radiative properties of water vapour have a strong influence on the overall composition and structure of the region. While the basic dynamical processes that govern the transport of water vapour throughout the UTLS are understood, important questions remain. For example, dynamical coupling between the stratosphere and troposphere via Stratospheric Tropospheric Exchange (STE) and the subsequent changes to distributions of the trace species, such as water vapour and ozone, are believed to result in a radiative feedback in the UTLS. This feedback has been shown to influence the formation of the Tropopause Inversion Layer (TIL) [4], a layer of enhanced static stability just above the tropopause that provides a barrier to vertical motions. Detailed structure has also been observed in the Tropical Tropopause Layer (TTL) that is not well understood. In addition, radiative feedback mechanisms associated with water vapour have been identified as a major source of uncertainty in current climate models.

Resolving these questions requires instruments capable of resolving spatial variations in the vertical distribution of the water vapour near the tropopause [4]. These variations have scales on the order of ~500 m [4]. Currently, the highest vertical resolution space based observations of UTLS water vapour are achieved using limb viewing sensors. Limb viewing satellites in a low-earth orbit provide the best combination of vertical resolution and global coverage. For example, the Michelson Interferometer for Passive Atmospheric Sounding (MIPAS) [5,6], the Atmospheric Chemistry Experiment (ACE) [7], the Scanning Imaging Absorption Spectrometer for Atmospheric CHartographY (SCIAMACHY) [8] and the Microwave Limb Sounder (MLS) on NASA's EOS Aura satellite [9] all provide between 3 and 5 km vertical resolution observations of the water vapour profile in the UTLS.

Limb observations are also conducted from stratospheric balloon and high altitude aircraft. For example, aircraft observations from the Gimbaled Limb Observer for Radiance Imaging of the Atmosphere (GLORIA) instrument [10,11] have provided measurements of the UTLS water vapour profile (as well as other important trace species) with a vertical resolution of <500 m in the 4 km – 20 km range [12]. It was shown that appropriate flight patterns can

* Corresponding author.
*E-mail address:* jeff.langille@usask.ca (J.A. Langille).

https://doi.org/10.1016/j.jqsrt.2018.01.026
0022-4073/© 2018 Elsevier Ltd. All rights reserved.

be chosen to facilitate three dimensional tomographic retrievals [13]. On the other hand, limb measurements from stratospheric balloons provide similar vertical resolutions and allow the in situ variability of the water vapour profile to be examined [14].

The Spatial Heterodyne Observations of Water (SHOW) instrument is a Canadian-led instrument concept that was initially developed at York University and is being further developed at the University of Saskatchewan in collaboration with ABB and the Canadian Space Agency (CSA) [15]. The instrument is being designed to provide high vertical resolution (< 500 m) observations of the UTLS water vapour profile from a satellite platform. This is achieved by combining an anamorphic imaging system with a spatial heterodyne spectrometer (SHS) [16,17] to observe limb scattered radiation in a narrow passband within a vibrational band of water (1363 nm–1366 nm) centred at ~1364.5 nm. Vertically resolved images of the water vapour spectra are obtained for each limb image. These images are then inverted to obtain vertically resolved measurements of the water vapour profile using standard inversion techniques [18].

A prototype instrument has been developed and tested as part of a CSA advanced space studies project and the performance of this design has been validated in the lab [15] using a water vapour cell to mimic several expected atmospheric water vapour pressures in the 8–40 km altitude range. The performance of the instrument was shown to be acceptable for the measurement of atmospheric water vapour using limb-scattered sunlight. In 2014, the SHOW instrument flew on a stratospheric balloon launched from Timmins Ontario [19]. The instrument operated for several hours at a float altitude of 37 km. These observations were used to validate the instrument configuration and demonstrate the technical readiness of the instrument technique for further study.

During 2016–2017, the SHOW instrument configuration was optimized for integration on NASA's ER-2 aircraft by ABB Ltd in collaboration with the University of Saskatchewan [20,21]. From July 17–21, 2017, the SHOW instrument flew aboard the ER-2 aircraft from the Armstrong Flight Research Centre (AFRC), located at (34N, 118W), on several engineering and science flights. The data that was acquired during these flights is currently being processed and the results from these flights will be presented in a different publication.

In this paper, we focus on the simulation of limb scatter observations, conducted from a high altitude aircraft with SHOW. These simulations and the subsequent examination of the retrieval sensitivity provides the ability to assess and refine the retrieval technique and determine the expected sensitivity to water vapour variability from a high altitude aircraft. A simulated 3D water vapour field has been provided by Environment and Climate Change Canada (ECCC) from the GEM-MACH (Global Environmental Multi-scale - Modelling Air quality and CHemistry) forecast model [22] to represent realistic variations in the water vapour profile along the flight path of the aircraft.

The paper provides an overview of the SHOW measurement technique and describes the forward model that is used to simulate limb scattered radiance and the instrument model used to simulate the realistic measurements. The retrieval technique is described and its application to SHOW limb measurements is discussed. The forward model, instrument model and retrieval implementation form a full model of the measurement process. This model is used to examine sensitivity of SHOW retrievals using realistic measurements. Finally, observations are simulated along a hypothetical flight path where the ER-2 flies at a constant altitude of 22 km and a constant speed of 800 km/h. These simulations are used to examine the spatial and temporal sampling capabilities of the instrument. It is shown that the sensitivity and sampling capability achieved by the instrument will allow for the small-scale gradients in the vertical distribution of the water vapour profile near the tropopause to be resolved.

## 2. SHOW ER-2 limb imaging configuration

The SHOW viewing geometry and mounting inside the ER-2 aircraft wing-pod are shown in Fig. 1(a) and (b) respectively. The optical layout of the instrument is shown in Fig. 1(c). The field of view looking out the wing pod window is ~4° in the vertical (4° downward from the boresight tangent) and 5° in the horizontal. This geometry is achieved by tilting the instrument downward inside the wing pod. The Figure shows a nominal aircraft altitude of 20 km and an example line of sight corresponding to the ~8 km tangent point. In practice, the aircraft altitude and pitch varies as a function of time and the lines of sight are defined using the aircraft attitude information.

The SHOW instrument combines an SHS with an anamorphic imaging system, operating in limb viewing mode, in order to obtain vertically resolved limb images of the water vapour absorption spectra in a narrow spectral window from 1363 nm to 1366 nm with an un-apodized spectral resolution of ~0.03 nm. The configuration and operation of an SHS is quite similar to a traditional Fourier Transform Spectrometer (FTS) such as a plane mirror Michelson (with a beam splitter and two plane mirrors) interferometer; however, the plane mirrors are replaced with fixed, tilted diffraction gratings. In the case of the SHS, a wavenumber dependent shear is introduced between the wave fronts exiting the interferometer. An image of the associated wavenumber dependent Fizeau fringes is formed by imaging the plane of the gratings onto a detector array. The gratings are operated in the Littrow configuration so that the fringes are heterodyned about the Littrow wavelength. A more detailed description of the SHS approach is given in [16].

The SHOW fore optics have an anamorphic design so that the limb is imaged in the vertical and defocused in the horizontal to provide a homogeneous scene in the interferogram dimension. This configuration has been chosen so that spatial variations in the horizontal limb radiance do not influence the spectral content recorded in the horizontal dimension at the detector. The SHOW aft optics and SHS are configured so a spatial heterodyned interferogram is imaged conjugate to the vertically resolved image of the limb at the detector. This provides a one-to-one mapping of tangent altitude to each row, i.e. each interferogram.

An example forward modelled SHOW limb measurement is shown in Fig. 2. The interferogram row corresponding to the tangent altitude at 16.45 km is shown in Fig. 2(a). The full interferogram image is shown in Fig. 2(b) where each interferogram row corresponds to a particular tangent altitude at the limb. The vertical intensity profile in the interferogram image is associated the variation of the limb scattered radiance with altitude. Each interferogram row is processed separately using analysis and calibration techniques similar to those applied in FTS to obtain the water vapour spectra corresponding to each tangent altitude. The associated spectrum corresponding to the tangent altitude at 16.45 km is shown in Fig. 2(c). The target wavelength region from 1363 nm to 1366 nm is isolated using a narrow band filter located in the aft-optics. The shape of the filter transmission profile (shown as the dotted line in Fig. 2(c)) as a function of wavelength is evident in Fig. 2(c) and (d). The lower wavelength cut-off corresponds to the Littrow wavelength of the device. The slight increase in intensity above the transmission filter on the left hand side of the profile is due to aliasing of spectral information from the left side of Littrow into the right side of Littrow, which will be discussed in more detail in Section 3.2. The modelled limb image of the water vapour spectrum, shown in Fig. 2(d), is obtained by applying this process to each interferogram row. In practice, the resulting spectrum is

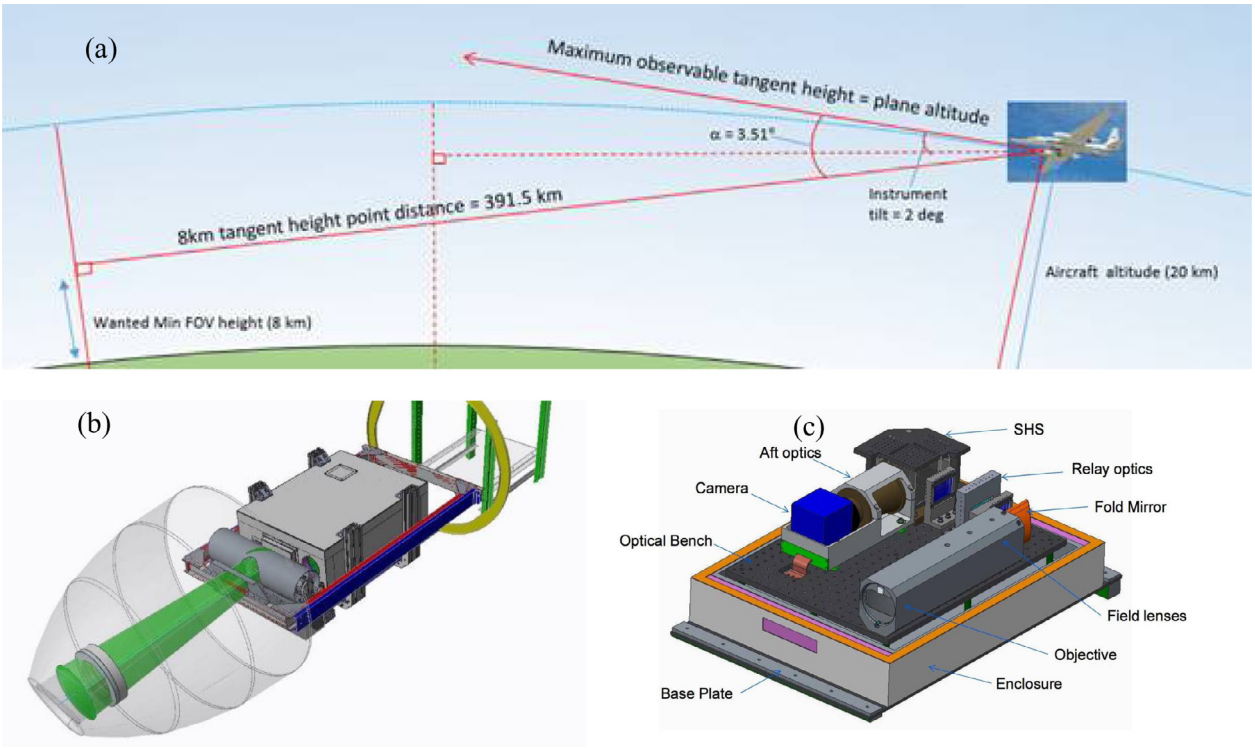


**Fig. 1.** SHOW ER2 viewing geometry (a), the SHOW instrument mounted inside the wing pod (b) of the ER-2 aircraft and the optical layout (c).

**Table 1**
SHOW ER-2 instrument parameters.

| Instrument parameter | Specification |
|---|---|
| ER-2 altitude | 22 km |
| Aircraft speed | ~800 km/hr |
| Field Of View | 4° vertical by 5.1° horizontal |
| Maximum angular vertical resolution | 0.0125° (1.7′) |
| Binned tangent point resolution (5 bins) | Approx. 500 m at 7 km<br>Approx. 200 m at 18 km |
| Mass | 269 lbs [122 kg] |
| Power | 465 W worst case, 200 W typical |
| Dimensions | (0.465 m × 1.32 m × 0.38 m) |
| Operating Temperature | −90 °C (at 60 kft altitude) to +40 °C |
| Spectral Resolution (theoretical) | ~0.03 nm |
| Along track sampling | ~200 m |
| Tangent point Vertical Resolution | ~100 – 500 m |

inverted using a non-linear retrieval algorithm coupled to the radiative transfer code and instrument model to obtain a vertically resolved water vapour profile. This is the topic of the next section.

Assuming an aircraft altitude of 22 km and a vertical field of view of 4°, the tangent points are located in the 6–21 km range. The raw SHOW images provide 320 vertical samples. This provides a maximum angular vertical resolution of 0.0125°. In the current implementation, the SHOW limb images are binned by row to provide 64 equally spaced vertical samples in this range. This provides a tangent point spatial sampling of approximately 500 m at 7 km and approximately 200 m at 18 km. An image of the limb is obtained every second (1 Hz sampling). Assuming an aircraft velocity of ~800 km/hr, this provides an along track spatial sampling of approximately ~ 200 m. The primary specifications of the SHOW flight instrument are summarized in Table 1.

## 3. Simulation and retrieval approach

A SHOW measurement simulator has been developed in Python to simulate SHOW limb observations from a high altitude aircraft platform. The simulator consists of the forward radiative transfer model (RTM), which is used to generate limb scattered radiances, the instrument model that simulates measurements from the high spectral resolution forward model spectra using the instrument properties, and the retrieval processor which is used to retrieve water vapour profiles from the observations. Although the simulations described in this paper are performed assuming an aircraft platform, the model is quite general and can be modified to simulate limb observations from a stratospheric balloon or a low-Earth orbit satellite.

### 3.1. Forward radiative transfer model

Realistic radiances are simulated using SASKTRAN [23]; a spherical radiative transfer model which solves the radiative transfer equation using the successive orders technique. For this study, we use a representative atmosphere consisting of water vapour, Rayleigh scattering, and stratospheric aerosol. The water vapour field is provided by an Environment and Climate Change Canada forecast model which is representative of expected atmospheric variability. An example of the simulated ECCC global distribution of water vapour at an altitude of 15.5 km is shown in Fig. 3(a). The two dimensional distribution along a longitudinal cut at 45W (black line in Fig. 3(a)) is shown in Fig. 3(b), which highlights the strong gradient near the tropopause and rapidly varying horizontal structure.

Absorption lines and corresponding line strengths are taken from the HITRAN 2008 database [24], and are both Doppler and collisional broadened. For the simulations, the pressure and temperature are taken from the MSIS-90 atmospheric model [25]. The stratospheric aerosol profile used is a typical tropical profile representative of 2016 conditions taken from the OSIRIS 5.07 data prod-

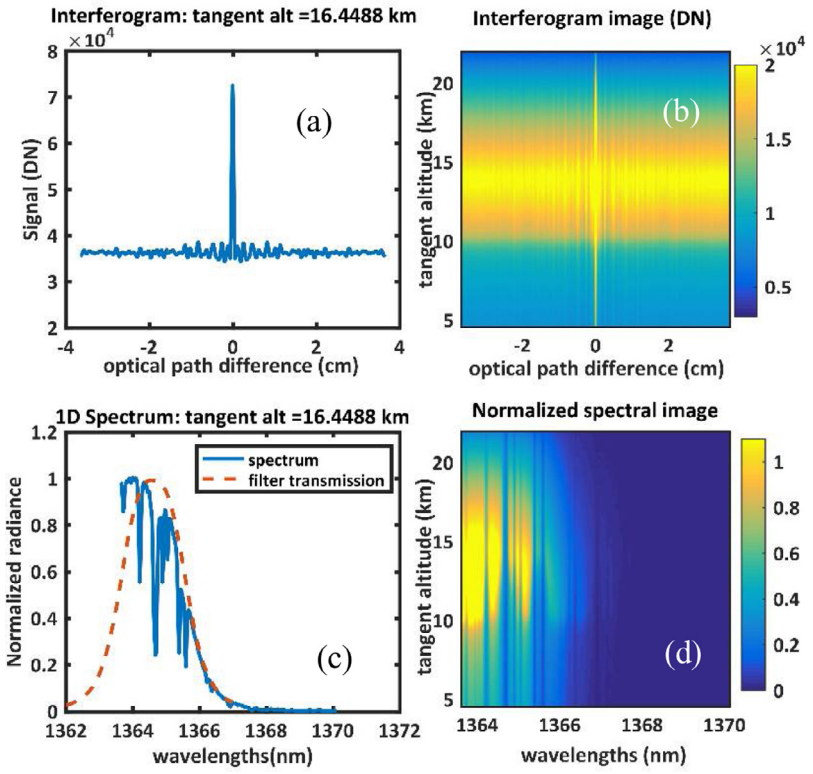


**Fig. 2.** Example SHOW modelled interferogram and spectrum. Interferogram row cut at the 16. 45 km tangent altitude (a) and the associated interferogram image (b) The corresponding one dimensional FFT at the 16.45 km tangent (c) and the associated spectral image obtained by performing a 1D FFT at each row (d).

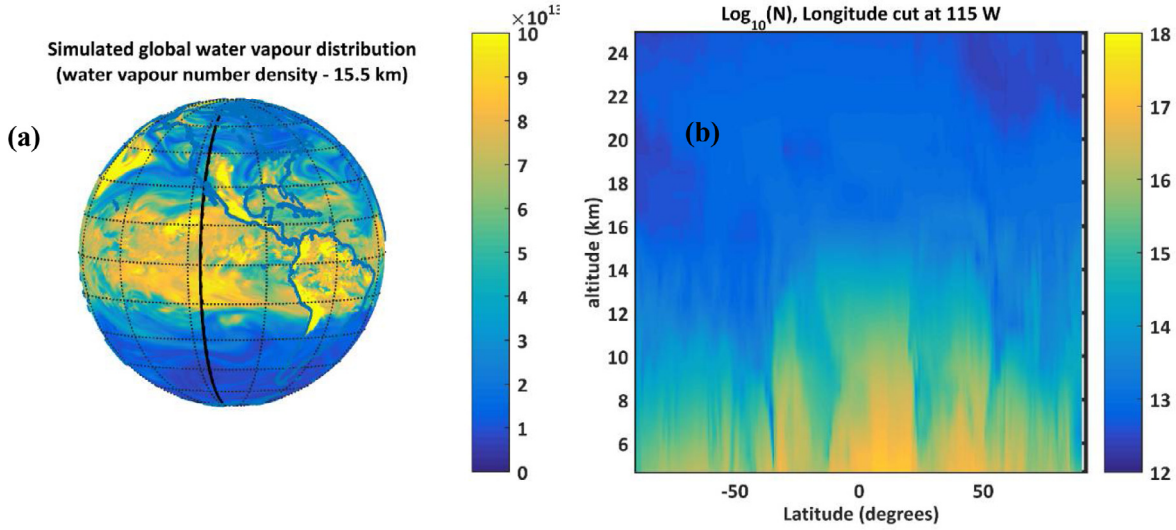


**Fig. 3.** Simulated global water vapour profile at 15.5 km altitude (a) and a cut along the 115W longitude line (b) shown as the black line on the global distribution.

uct [26]. Stratospheric aerosols are assumed to be $H_2SO_4$ particles following a log-normal size distribution with a mode width of 1.6 and a mode radius of 80 nm with scattering properties calculated with a Mie code.

SASKTRAN can be configured to handle the atmosphere in two different ways [27]. The first is a one- dimensional mode where the atmospheric constituents vary only in altitude. Here, the average latitude and longitude of the tangent point of the measurements is determined and each species climatology is selected at this point. The height resolution between atmospheric layers is a user input, and logarithmic interpolation is used between each layer. The second mode is a two-dimensional mode, where the atmosphere varies in both altitude and along the line-of-sight (horizontal) dimension. Divisions in the horizontal dimension are a user input with linear interpolation being performed between them. The altitude divisions and interpolation are done the same as the one-dimensional mode. Using the two-dimensional mode it is possible to perform tomographic retrievals [28]; however, for this study, we use the one-dimensional mode to perform both the forward modelling and retrievals.

To demonstrate the forward model, a high spectral resolution simulation of the limb-scattered spectral radiance within the SHOW instrument passband is performed. For the simulation, the observer is located at an altitude of 22 km and is positioned at a

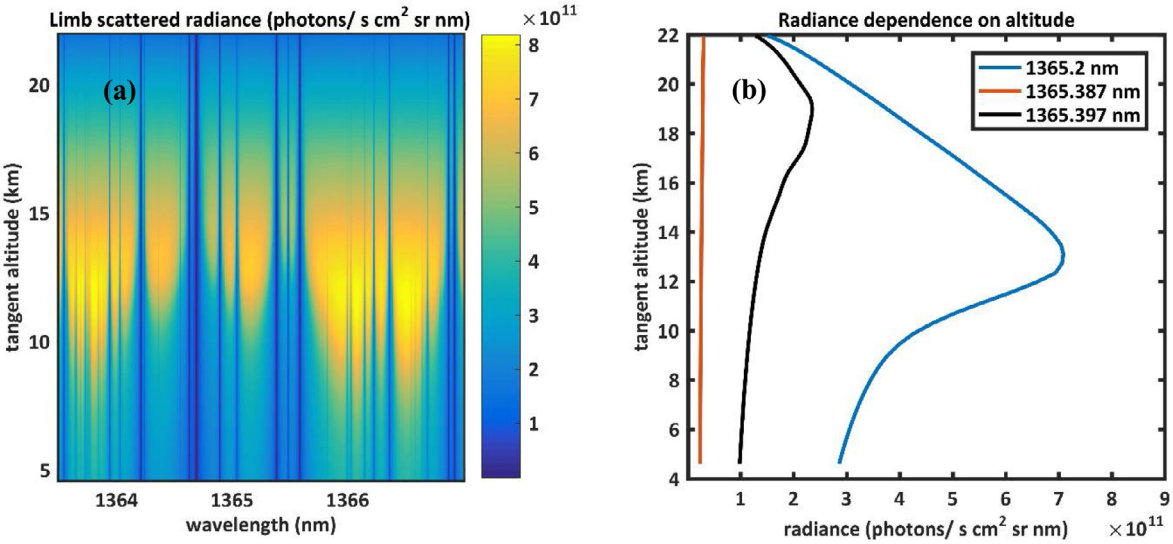


**Fig. 4.** High-resolution radiance profile as a function of altitude in the SHOW instrument passband (a) and the altitude dependence of the radiance profile at 1365.2 nm, 1365.387 nm and 1365.397 nm (b).

latitude and longitude of 28.55°N and 119.88°W, respectively. One thousand equally spaced wavelengths (0.0034 nm spacing), which is enough to resolve even the narrowest of lines in this spectral window, were computed within the SHOW passband at 64 tangent altitudes in the 4 km – 22 km region. The case of a single scatter and multiple scattering (3 scatters) model was examined. It was found that the single scatter case varied by less than 1% from the multiple scattering case. The reason that this is so small is because the tropospheric column of water vapour is so high that photon paths below the instrument lines of sight are essentially completely absorbed coupled with the fact that the Rayleigh and aerosol optical depths are very low in the near infrared. In addition, the single/multiple scatter difference between the two cases is uniform with altitude. In the present study, we utilize the single scattering case in order to speed up the radiative transfer calculations with essentially no effect on the results.

An example of the high-resolution spectral radiance as a function of wavenumber and altitude for the single scatter case is shown in Fig. 4(a). The individual water absorption lines can clearly be seen in the radiance profile. Brightness generally increases with decreasing altitude until approximately 12 km. At this altitude the absorption lines are collisional broadened enough that the entire spectral range is affected by water vapour absorption and it becomes optically thick at all wavelengths. The effect is observed more clearly in Fig. 4(b) which shows the radiance profile as a function of altitude at 1365.2 nm, a wavelength far from any absorption line (blue). The radiance rises with decreasing altitude due to rapidly increasing Rayleigh and aerosol scattering, and at ~13 km there is a sudden drop in the profile due to water vapour absorption in the wings of absorption lines. The radiance profile as a function of altitude at 1365.387 nm and 1365.397 nm, wavelengths located inside a strong absorption feature is also shown (red and black respectively), and a similar effect is observed at a much higher altitude. Clearly, the radiance profile varies less sharply close to the absorption feature.

The high-resolution spectra at several tangent altitudes within the SHOW field of view are shown in Fig. 5(a). At 17 km we see a relatively constant baseline scattering level with primarily Doppler broadened absorption lines. At 13 km we begin to see collisional broadening, but the baseline level is still visible between absorption features. At 7 km collisional broadening is the dominant effect, the entire range is affected by water vapour absorption and the intensity is decreased from the 17 km measurement. Fig. 5(b) and (c) show the same high-resolution spectra zoomed in on a weak and strong absorption feature respectively. For several weak absorption lines the depth of the lines increases with decreasing altitude, indicating that the depth of these lines contains useful information on the water vapour content. For the strong lines, the depth stays constant (fully absorbed) independent of altitude. For these lines, the information content is contained in the line shape.

### 3.2. Instrument model

The forward model provides the input radiance to the SHOW instrument model, which uses the theoretical framework developed by Harlander [16] to model SHOW interferogram images. The SHOW optical configuration and measurement approach was discussed in Section 2. At the detector, the limb is imaged conjugate to the spatial heterodyned fringes in the vertical dimension and each sample in the horizontal dimension of the interferogram averages over the horizontal scene (anamorphic design). Therefore, the spectral information is contained in the horizontal (x) dimension and the vertical (spatial) information is contained in the vertical (y) dimension of the detector. Each row on the detector is mapped one-to-one to a particular tangent point at the limb.

Following from [16], each interferogram row corresponding to each tangent point in the field of view is modelled using Eq. (1).

$$\boldsymbol{I}(\boldsymbol{x}) = \boldsymbol{q}tA\Omega \int_0^\infty \boldsymbol{\tau}(\boldsymbol{\sigma})\boldsymbol{B}(\boldsymbol{\sigma})\left[1 + \boldsymbol{M}\cos\left[2\boldsymbol{\pi}\left(4(\boldsymbol{\sigma} - \boldsymbol{\sigma}_0)\boldsymbol{x}\tan\left(\boldsymbol{\theta_L}\right)\right)\right]\right] \tag{1}$$

In this equation, $x$ is position on the grating, q is the quantum efficiency of the detector array, $B(\sigma)$ is the spectral limb radiance given by the forward model, $\sigma_0$ is the Littrow wavenumber, $\theta_L$ is the Littrow angle, $\sigma$ is the wavenumber, t is the exposure time, $A\Omega$ is the optical throughput defined by the area of a pixel times the solid angle subtended at the pixel, $\tau(\sigma)$ is the transmission of the system and includes the filter transmission ($\tau_f(\sigma)$) as well as the overall transmission of the optical system ($\tau_o(\sigma)$), and M is the modulation efficiency of the SHS. The gratings are tilted by the Littrow angle $\theta_L$ so that the spatial frequency of the interference fringes produced at the Littrow wavenumber corresponds to the zero spatial frequency fringe.

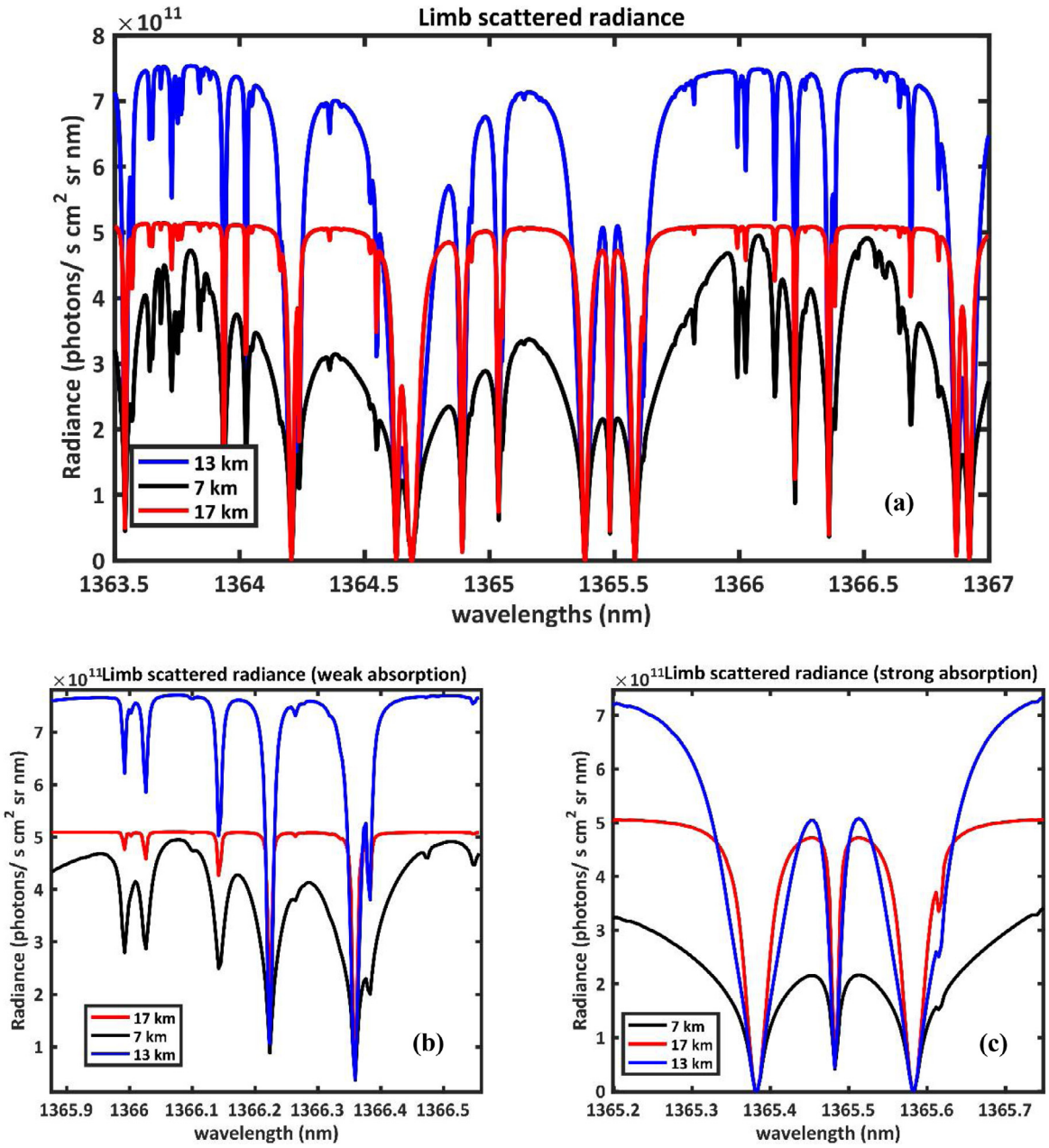


**Fig. 5.** Examples of absorption spectra over the full SHOW passband (a) and zoomed views of weak (b) and strong (c) absorption features within the SHOW passband.

In the work presented in this paper, Eq.(1) is used to model interferogram rows using the instrument properties listed in Table 2. The forward model discussed in the previous section is used to simulate the limb radiance $B(\sigma)$ for each tangent altitude. A double-sided interferogram row is modelled for each corresponding tangent altitude. Poisson noise associated with photon counting, readout error and dark signal is added to the detected photon signal recorded at each pixel in the interferograms. The associated error on the measured spectral signal is estimated using the approach described in [29].

Procedures that are analogous to the traditional FTS techniques are utilized to extract spectra from each row of the resulting image. This includes the removal of DC bias and the application of Apodization using a Hanning function. An FFT is used to determine the amplitude of the complex spectrum for each row of the interferogram image. The result is a vertically resolved image of the limb scattered sunlight spectra containing the water vapour absorption lines. The number of spectral samples provided by the FFT (without zero padding) is set by the Nyquist limit, whereas, the maximum spectral resolution is set by the maximum optical path difference of the SHS [16]. The SHOW design provides 256 spectral samples and a maximum theoretical spectral resolution of ~0.03 nm.

It is important to point out that the current study does not deal with several important non-ideal instrument effects. For example, one of the primary advantages of the SHS technique over the FTS approach is that the interferogram is obtained in a single frame without scanning. This allows for higher sampling rates and a less complicated instrument; however, each pixel in the interferogram row now acts as a separate detector. In practice, this means that inter-pixel intensity variations, non-ideal flat fields, phase distortions, and the presence of bad, hot or dead pixels will lead to er-

**Table 2**
SHOW ER-2 SHS instrument specifications.

| Specification | Value |
|---|---|
| $A\Omega$ (per pixel) | $0.836 \times 10^{-6}$ cm$^2$sr |
| M | 0.9 |
| $\tau_f$(peak) | 0.775 |
| $\tau_o$ | 0.294 |
| t | 300 ms |
| $\theta_L$ | 28.5° |
| W (width of imaged portion of grating) | 3.73 cm |
| Littrow wavelength | 1363.63 nm |
| FPA dimensions (Raptor OWL 640) | $512 \times 640$ (15 µm pixels) |
| Gain | 39.67 electrons/DN |
| Readout Noise | 195 electrons |
| Quantum efficiency | ~0.85 |
| Dark current (0 C) | 5000 electrons/s |

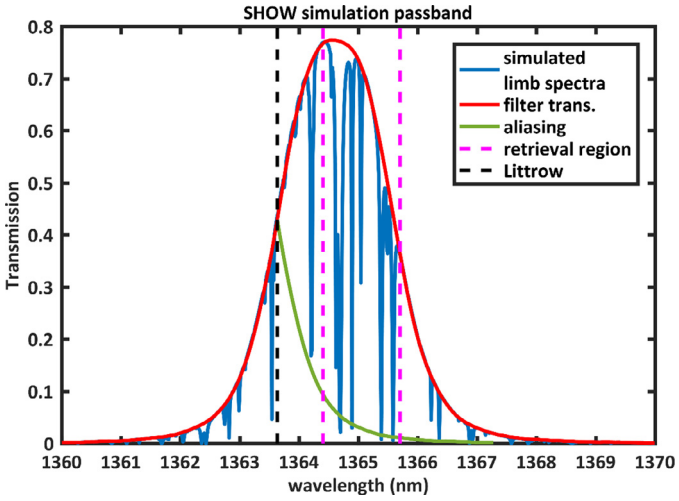


**Fig. 6.** The SHOW passband utilized in the instrument model.

rors in the returned spectrum. For the flight instrument, calibration procedures such as those discussed in [30,31] will be applied to characterize these effects and minimize their impact on the measurements.

Another important practical consideration is the sensitivity of the measurements to temperature changes. The SHOW SHS is not thermally compensated; therefore, the Littrow wavelength of the device varies with temperature (ref. [15]). Although the temperature of the flight instrument will be actively controlled, smooth variations in the Littrow wavelength with temperature are expected. Errors in the knowledge of the Littrow wavelength will lead to errors in the locations of the water vapour absorption lines. Since the observed spectrum contains well-known spectral features, the Littrow wavelength will be tracked during the flight by including the Littrow wavelength as a free parameter in a fit to the observed spectrum.

Also, observe from Eq. (1) that signals that are separated by the same amount on either side of Littrow are indistinguishable. Subsequently, spectral information from the left side of Littrow is aliased into the right side. Ideally, the impact of aliasing is minimized by designing the filter such that the Littrow wavelength is located close to the edge of the passband, therefore, reducing the amplitude of the aliased signal to a negligible level. The transmission profile of the SHOW filter is shown in Fig. 6 plotted (red) overtop of a forward modelled high-resolution limb spectrum (blue). The black dotted line identifies the location of Littrow wavelength within the SHOW passband and the purple dotted lines identify the wavelength range that is utilized by the retrieval (from 1364.6 nm to 1365.7 nm). The Littrow wavelength of the SHOW ER-2 instrument is approximately 1363.63 nm, therefore, the filter transmits signals from the left side of Littrow. The magnitude of the aliased portion of the filter transmission function is shown in green in Fig. 6. The aliased signal is $<$ 10% at 1364.6 nm, $<$ 5% at 1364.7 nm and $<$ 1% at 1365.7 nm. These signals have a negligible impact on the simulated retrievals presented in this paper.

### 3.3. Retrieval algorithm

The technique that is utilized for SHOW retrievals is based on the non-linear optimal estimation approach developed by Rodgers [18]. This is a general inversion approach that is widely utilized in passive atmospheric remote sensing applications [8,12]. The goal of the retrieval processor is to find the best representation of the water vapour profile, or state vector, $x$, given a set of measurements, $y$, and additional a priori information. The variables x, y must not be confused with the geometrical coordinates in Eq. (1). Here x, and y are used since they are the traditional notation used in the literature. In this case, the measurements correspond to the vertically resolved water vapour spectra obtained using the SHOW measurement approach.

In this paper, we follow the framework presented in [18] and perform the iterative step,

$$\boldsymbol{x_{i+1}} = \boldsymbol{x_i} + \left(\boldsymbol{K^T S_y^{-1} K} + \boldsymbol{R} + \lambda \boldsymbol{I}\right)^{-1} \{\boldsymbol{K^T S_y^{-1}}[\boldsymbol{y} - \boldsymbol{F}(\boldsymbol{x_i})] - \boldsymbol{R}(\boldsymbol{x_i} - \boldsymbol{x_a})]\}, \tag{2}$$

where $i$ is the iteration number, $K$ is the Jacobian matrix, $S_y$ is the measurement error covariance matrix, $R$ is a regularization matrix, $\lambda$ is a Levenberg-Marquardt [32] type damping parameter, $F$ is the forward model, and $x_a$ is an a priori state vector. The gain matrix is defined as,

$$\boldsymbol{G} = \left(\boldsymbol{K^T S_y^{-1} K} + \boldsymbol{R}\right)^{-1} \boldsymbol{K^T S_y^{-1}}, \tag{3}$$

which allows us to calculate the measurement error component of the solution covariance,

$$\boldsymbol{S_{random}} = \boldsymbol{G^T S_y G}, \tag{4}$$

and the averaging kernel,

$$\boldsymbol{A} = \boldsymbol{GK}. \tag{5}$$

The measurements used in the retrieval are the logarithm of the high altitude normalized spectra for the entire spectral window, i.e.,

$$\boldsymbol{y_{ij}} = \boldsymbol{log}\left(\frac{\boldsymbol{I}(\lambda_i,\ \boldsymbol{h_j})}{\boldsymbol{I}(\lambda_i,\ \boldsymbol{h_{norm}})}\right), \tag{6}$$

where $h_{norm}$ is the tangent altitude of the highest possible altitude measurement, which practically for the aircraft viewing geometry is about 2 km below the flight altitude. The logarithm of the spectrum is taken due to the tendency of limb scattered radiance to increase exponentially with a decrease in tangent altitude. The high-altitude normalization is included both to reduce calibration issues and to remove the dependency on knowledge of the incoming solar flux. It also avoids retrieval of negative values for water concentrations in the case of noisy data.

The state vector, $x$, used is the logarithm of $H_2O$ number density at a set of discrete altitudes. Through testing it was found that the retrieval was closer to the linear regime when performed in log space. It is important to note that internally, the forward model performs linear interpolation of the state vector between the discrete altitudes it is specified at, and thus the state vector must be interpreted this way. Rather than attempting to choose the vertical spacing of the retrieval grid to match the information content of the measurements, we use a finely spaced retrieval grid of 250 m

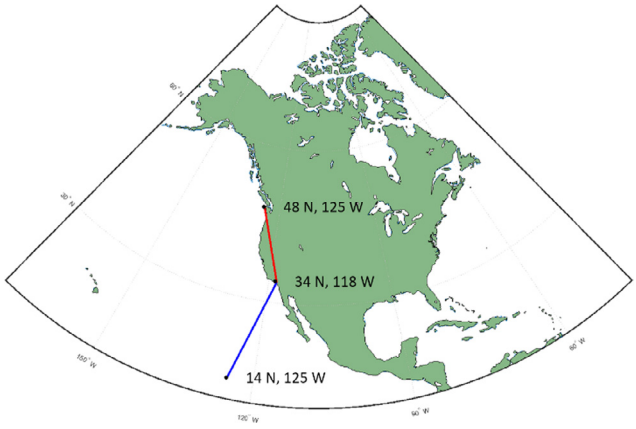


**Fig. 7.** SHOW ER2 simulation flight path.

and let the amount of regularization control the vertical resolution. A Tikhonov type constraint is included as the regularization matrix,

$$\boldsymbol{R} = \gamma \boldsymbol{L}_2^T \boldsymbol{L}_2, \tag{7}$$

where $L_2$ is a second order difference operator and $\gamma$ is a parameter that controls the amount of regularization. The effects of the included regularization is discussed in later sections.

The upper and lower altitude limits of the retrieval are determined by the measurement sensitivity to the water vapour at those altitudes. At high altitudes the water density decreases rapidly to the point where there is too little to measure. This optically thin region produces weak spectral signals that will reduce the overall accuracy of the retrieval. Similarly, at low altitudes the water density increases rapidly and the region becomes too optically thick to see the tangent point. In testing, it was found that a robust high altitude limit could be found at 18 km but the low altitude limit is much harder to set due to the large variability in the water vapour optical depth.

In an attempt to dynamically determine this lower limit, every iteration of the retrieval examines the Jacobian matrix to determine the altitude below which the measurements cease to be useful. The Jacobian contains information regarding how sensitive the measurements are to changes in the water profile. If a measurement is appropriately sensitive at a particular altitude, then a perturbation at that altitude should have the largest affect on the measurements at this height. To set the lower altitude limit, only measurements that are maximally sensitive to changes in the water vapour profile at the tangent point are used. This results in a lower altitude boundary on the retrieval that varies between 8 and 13 km.

## 4. SHOW measurement simulations

The forward model, instrument model and retrieval processor described in the previous sections form the core of the SHOW measurement simulator. The goal of the SHOW ER-2 measurement simulations is to validate the retrieval approach and demonstrate the sensitivity and the spatial sampling capabilities from an aircraft. This is achieved by simulating SHOW measurements from an aircraft flying at 22 km, assuming a hypothetical flight track (see Fig. 7) from (34N,118W) to (48N,125W) on a North line, and from (34N,118W) to (N 14, W 125) on a South line. Realistic signals, including measurement noise (Poisson) are modelled using the SHOW measurement simulator.

The simulations presented here assume that the flight path of the ER-2 aircraft is linear and that the altitude is constant at 22 km. In practice, the aircraft pitch will vary as a function of time as the aircraft porpoises up and down along the flight track. This results in a particular tangent point being viewed by a small range of rows as a function of time. This must be corrected to avoid the smearing of radiance information across rows. For the SHOW ER-2 measurements, the aircraft will fly at a fixed altitude and direction. In this case, the pitch variation is expected to be smooth relative to the 1 Hz sampling rate of the SHOW instrument. Such a variation results in interferometric DC signals that are well-correlated with the pitch variation. In practice, this correlation will be used to correct the interferograms for the aircraft pitch variation and obtain a one-to-one mapping of tangent altitude to interferogram row. Such variations are neglected in the current study.

The simulated water vapour profile provided by ECCC has a 1 km vertical resolution, a 0.225° latitude resolution and a 0.351° longitude resolution. Therefore, the simulated flight corresponds to 100 equally spaced samples taken every 29 km along the flight track. This is much lower than the expected along track sampling of the ER-2 flights ($\sim$ 200 m); however, it is matched to the forecast model water vapour field without interpolation. In some cases, the vertical structure in the model water vapour profile is sharply discontinuous. In these cases, the profiles were smoothed to remove the discontinuities.

The measurement simulator does not include clouds. In practice, scattering from clouds results in saturated signals at the centre burst of the SHOW interferograms. This results in charge spilling over into other pixels, which subsequently corrupts the images. Measurements that are obtained during an actual flight will need to be examined for the presence of clouds and removed from the processing chain.

Assuming a field of view of 4°, the image of the limb fills 320 vertical bins in the observed FOV on the SHOW detector array. This provides a maximum angular vertical resolution of 0.0125°. For the current configuration, each frame is binned by 5 rows in order to increase the SNR and decrease the processing time. This provides 64 vertical bins corresponding to 64 tangent altitudes with a 0.0625° vertical resolution. Therefore, the measurement vector corresponds to 64 tangent altitudes and each tangent altitude has 256 spectral samples.

Integration times were chosen so that the central peak of the interferogram is below saturation for all measurements. This corresponds to an integration time of 300 ms which provides a spectral SNR between 250 and 600, with the upper value corresponding to the SNR of the continuum close to the tropopause. The amount of smoothing was adjusted to obtain the best vertical resolution possible using this SNR.

### 4.1. SHOW ER-2 flight simulation

The results from the full flight simulation are shown in Fig. 8. The true water vapour profile is shown in Fig. 8(a), the retrieved water vapour profile is shown in Fig. 8(b) and the error (taken as the difference between the true and retrieved profile) is shown in Fig. 8(c). A significant amount of variability is observed in the water vapour profile along the flight path. This variability is resolved by SHOW in the region between 12 and 18 km with $< \pm 1$ ppm error in the measurements.

The white region in Fig. 8(b) and (c) corresponds to the lower altitude cut-off which is determined using the approach discussed in the previous section. On average, the simulated retrieval fails below 12 km where the atmosphere becomes optically thick. Above 18 km, the path length between the instrument and the tangent point is too small, making retrievals difficult at these altitudes. The lower altitudes where the atmosphere has become optically thick are identified as the sharp cut-off regions shown in white in Fig. 8(b). In some cases, the approach that is used to identify the

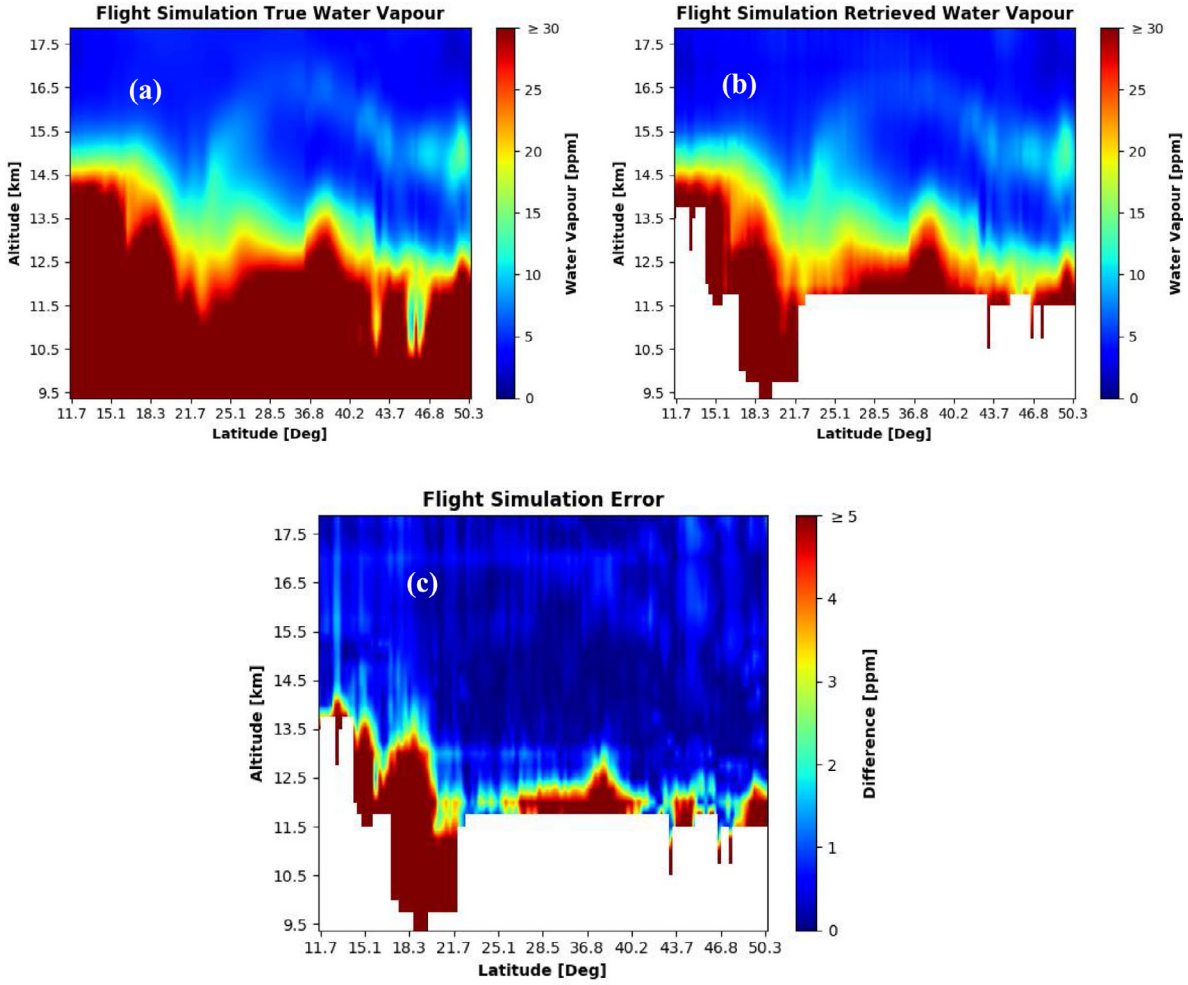


**Fig. 8.** SHOW ER-2 flight simulation. True water vapour profile (a), the retrieved water vapour profile (b) and the difference between the true and retrieved profiles (c) as a function of latitude.

valid retrieval region doesn't work properly. For example, the retrieval at ~ 18–21° latitude appears to extend down to ~ 9.5 km. A quick comparison with the error plot in Fig. 8(c) shows that the retrieval does not produce accurate results at these altitudes (> 25% error). This effect is due to the fact that the technique used to identify the optically thick region is only approximate, and in some cases, does not properly set the lower boundary of the retrieval. Regardless, the retrieval still produces reasonable results from 12 to 18 km.

Several aspects have an influence on the sensitivity of SHOW limb measurements. For example, measurement noise and the use of smoothing via Tikhonov regularization has a significant impact on the measurement error, as well as, the vertical resolution of the measurements. In practice, one is a trade off against the other and an appropriate amount of smoothing must be determined given the specific SNR of the measurements. Increasing the amount of smoothing degrades the vertical resolution and improves the uncertainty of noisy data. Another aspect that influences the retrieval is the state of the atmosphere. For example, the presence of strong gradients in the water vapour profile has the potential to be problematic when the vertical resolution is reduced [see ref.8 for example]. In addition, differences between the amount of aerosol used in the retrieval and the amount of aerosol used in forward modelling may also influence the retrieval. Each of these cases will be examined in the next several sections.

### *4.2. Sensitivity to water vapour*

A typical water vapour profile retrieval corresponding to the measurement at a reference latitude of 38.8° is shown in Fig. 9(a). The corresponding averaging kernel plotted as a function of altitude is shown in Fig. 9(b). The measured spectral image and the associated SNR of the measurements is shown in Fig. 10(a) and (b) respectively. The SNR of the measurements ranges from 200 to 600 within the SHOW passband.

Observe that the retrieval converges in several iterations and performs well from ~12 km up to ~18 km. Also, observe that the different colours in Fig. 9(b) correspond to the averaging kernels associated with each tangent point and that the averaging kernels peak close to the tangent points. In addition, the measurement response function, which is taken to be the sum of the averaging kernels, is close to one from 13 km up to 18 km (black dotted line). This confirms that the information content of the retrieval is not strongly influenced by the a priori in this altitude region. Below 13 km, the measurement response function goes through a sharp increase and then rapid decrease towards zero. This corresponds to the fact that retrieval is not well-behaved where the atmosphere becomes optimally thick. Accordingly, larger retrieval errors also become evident at the same altitude. The approximate vertical resolution of the measurements, estimated from the full width half maximum of the averaging kernel at each tangent altitude varies from ~650 m down low to ~850 m up high.

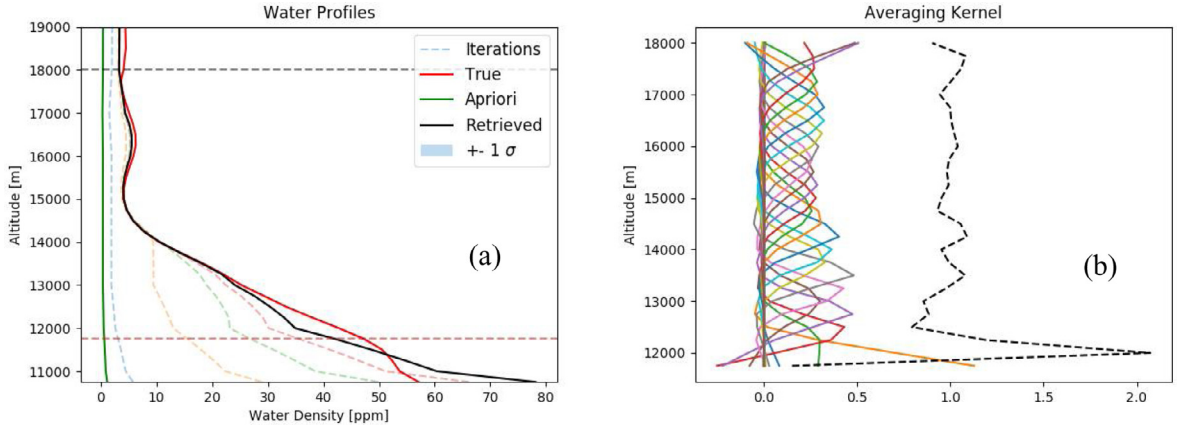


**Fig. 9.** Simulated water vapour retrieval at a latitude of 38.8° (a) and the associated averaging kernel (b) The +/−sigma bands that are shaded in blue correspond to the retrieval measurement precision and are too small to be seen. (For interpretation of the references to colour in this figure legend, the reader is referred to the web version of this article.)

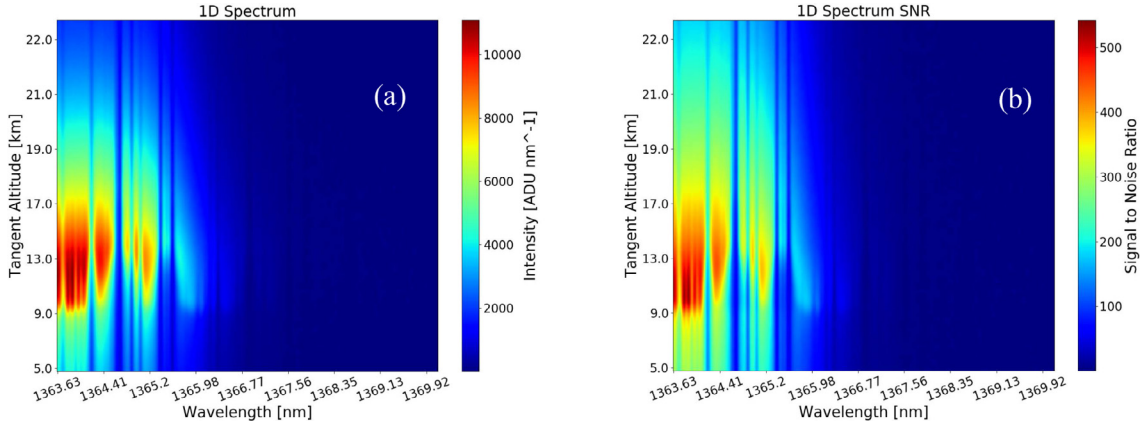


**Fig. 10.** Example of the SHOW spectra (a) and the associated SNR (b) associated with the simulated measurement used in the retrieval shown in Fig. 8.

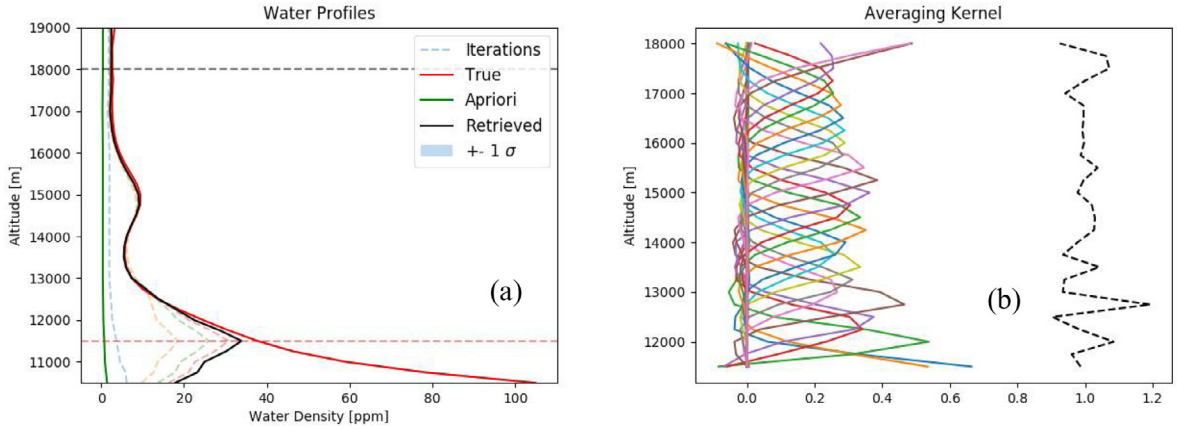


**Fig. 11.** Simulated water vapour retrieval at a latitude of 47.97° (a) and the associated averaging kernel (b) The +/−sigma bands that are shaded in blue correspond to the retrieval measurement precision and are too small to be seen. (For interpretation of the references to colour in this figure legend, the reader is referred to the web version of this article.)

A second example retrieval and corresponding averaging kernel is shown in Fig. 11. Here the reference latitude is 47.97°. In this case, this water profile exhibits slightly stronger gradients with altitude. Again, the retrieval converges in several iterations and is well-behaved between ~12 km and ~18 km. The averaging kernels are also well-peaked at the tangent altitudes. In this case, the measurement response function is close to one down to 11.5 km. Below 11.5 km, the atmosphere becomes optically thick and the retrieval fails. In this example. the vertical resolution, taken to be the full width half maximum of the averaging kernels varies from ~ 650 m down low to 900 m up high.

The vertical resolution of the SHOW instrument can be increased by increasing the SNR of the measurements while keeping the amount of smoothing applied in the retrieval constant. This can be achieved by taking longer exposures or by averaging successive images. In this case, the vertical resolution is increased at

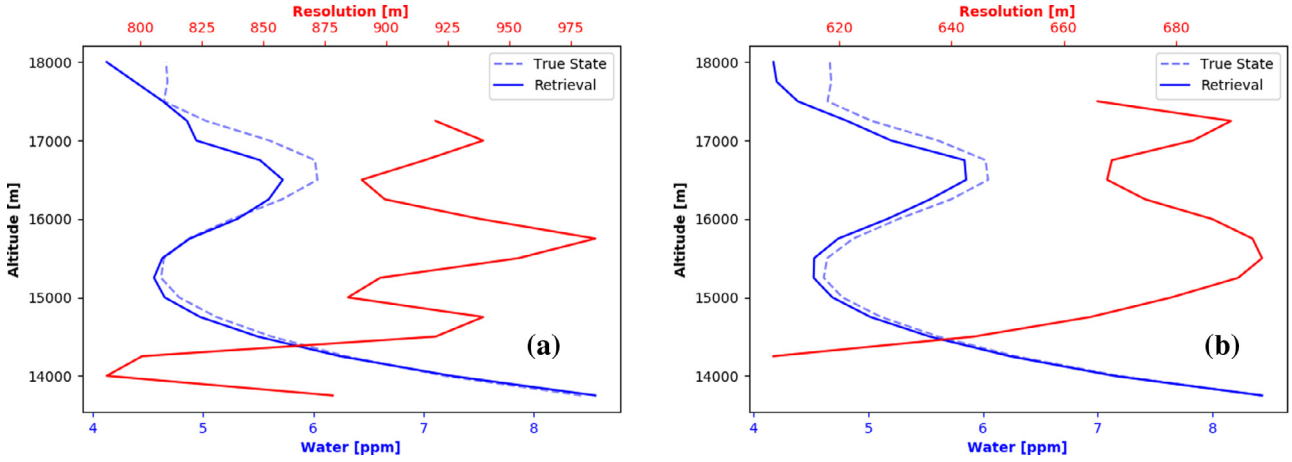


**Fig. 12.** An example water vapour profile and approximate vertical resolution in the case where the SNR is given in Fig. 8(a) and the case where the SNR is increased by a factor of $\sqrt{5}$ (b).

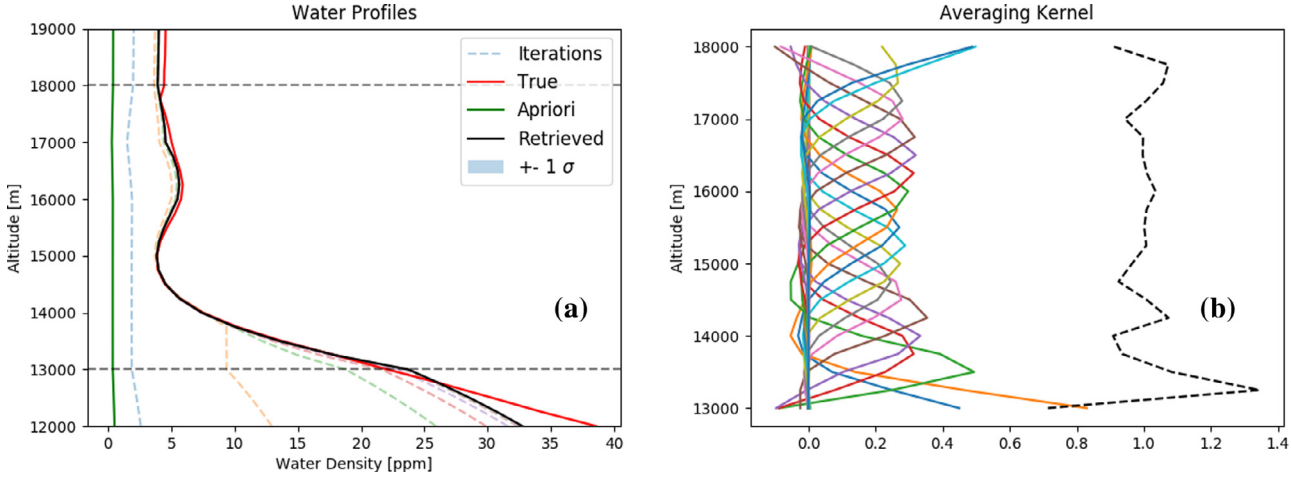


**Fig. 13.** Baseline retrieval used to examine the impact of changes to the a-prior aerosol profile. The +/- sigma bands that are shaded in blue correspond to the retrieval measurement precision and are too small to be seen. (For interpretation of the references to colour in this figure legend, the reader is referred to the web version of this article.)

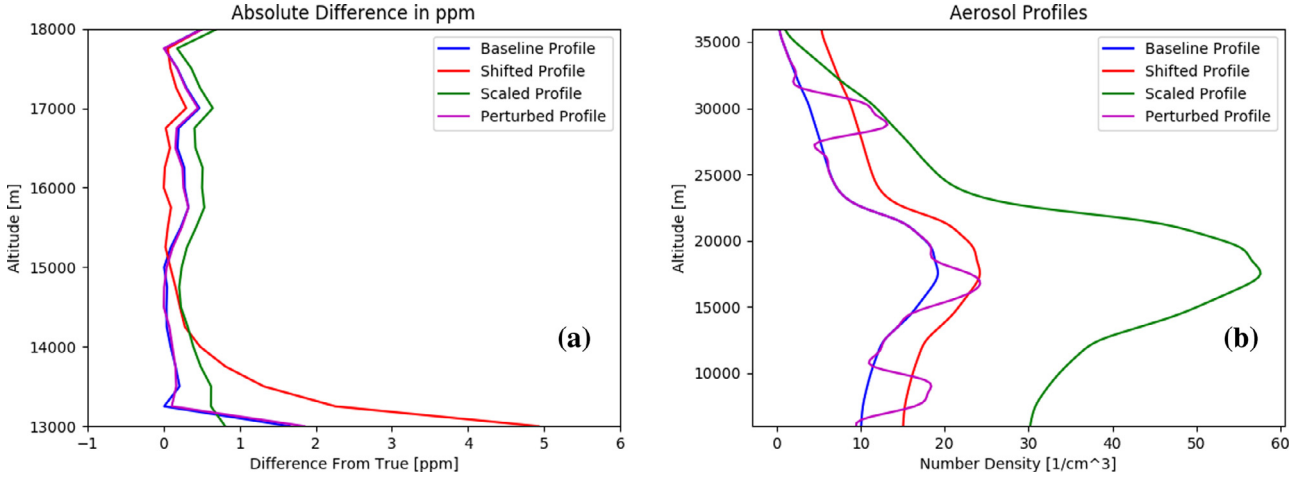


**Fig. 14.** Sensitivity to the amount of aerosol. Absolute difference between the true and retrieved profile (a) using the different a priori aerosol profiles shown in (b).

the expense of the horizontal resolution of the along-track sampling. As an example, 5 images are averaged together in order to increase the SNR by a factor of $\sqrt{5}$. Fig. 12(a) and (b) shows the retrieved water vapour profile and associated vertical resolution in both cases. Using this increased SNR, the vertical resolution is increased from between 775 m and 1000 m to between 600 m and 700 m for all retrieval altitudes.

### 4.3. Sensitivity to aerosol

In general, knowledge of the amount of aerosol present in the atmosphere provides a more accurate forward model. In practice, one does not know the actual amount of aerosol in the observed atmosphere and the local amount of aerosol present at any particular location can vary significantly over time. For the SHOW re-

trievals, an a priori profile was chosen that is representative of the tropical aerosol extinction profile taken from the OSIRIS v5.07 dataset [26].

The impact that differences between the true aerosol amount and the a priori aerosol amount used for forward modelling on the retrieved water vapour profile has been examined for several specific cases. These include the impact of a shift, scale and change to the shape of the measurement aerosol profile relative to the a priori. The baseline retrieval that is used for this study corresponds to the simulated measurement taken at 36.49N (see Fig. 8). The retrieval and associated averaging kernel that is used for this measurement is shown in Fig. 13(a) and (b) respectively. The retrieval performs well between 13 km and 18 km and the behaviour of the retrieval is similar to the behaviour exhibited by the retrievals discussed in the previous section. Again, the lower altitude cut-off corresponds to the case where the atmospheric has become optically thick (see Section 3.3).

Fig. 14(a) shows the absolute difference in ppm between the true and retrieved water vapour profile for the various a-prior aerosol profiles shown in Fig. 14(b). In all cases, differences between the a priori and measurement aerosol profiles result in only slight changes ($<$ 1 ppm) to the retrieved water vapour profile in the retrieval range from 13 km to 18 km.

## 5. Summary and conclusion

The SHOW instrument is a Canadian led prototype satellite instrument that is being developed at the University of Saskatchewan in collaboration with ABB ltd and the Canadian Space Agency to measure the vertical distribution of water vapour in the UTLS region. The instrument has been optimized for observations from a high altitude aircraft, specifically, the ER-2 aircraft operated by NASA at AFRC, CA.

A SHOW measurement simulator has been developed in Python that incorporates a forward model, an instrument model and the retrieval processor. This simulator was used to simulate 100 equally spaced measurements from an aircraft flying at 22 km on a hypothetical flight track from (34N,118W) to (48N,125W) on a North line and (34N,118W) to (N 14, W 125) on a South line. A modelled global water vapour distribution was used to provide realistic variability in the water vapour profile along the flight path.

The work presented in this paper demonstrates the sensitivity and sampling capabilities of the SHOW measurement technique assuming realistic signal levels and an ideal instrument behaviour. It was shown that the sensitivity of the SHOW retrievals is primarily limited by the SNR of the measurements and the amount of regularization applied. The behaviour of the retrieval processor is similar across the full flight track and the vertical resolution of the measurements can be increased at the expense of the along track sampling. The a priori aerosol profile was shown to have a negligible impact on the retrieval processor.

Operating from an aircraft platform flying at 22 km, the instrument is capable of achieving 500 m–1 km vertical resolution in the 12 km – 18 km region with $< \pm 1$ ppm accuracy (assuming a 1 Hz sampling rate). Therefore, SHOW is capable of resolving the variability in the UTLS water vapour profile and provides better or equal spatial resolution and accuracy in comparison to other techniques [5–14].

## Supplementary materials

Supplementary material associated with this article can be found, in the online version, at doi:10.1016/j.jqsrt.2018.01.026.

## References


[1] Gettelman A, Hoor P, Pan LL, Randel WJ, Hegglin MI, Birner T. The extratropical upper troposphere and lower stratosphere. Rev Geophys 2011;49.

[2] Sherwood SC, Roca R, Weckwerth TM, Andronova NG. Tropospheric water vapour, convection, and climate. Rev Geophys 2010;48.

[3] Seinfeld and Pandis, Atmospheric chemistry and physics: from air pollution to climate change, second ed., 2006.

[4] Randel WJ, Jensen EJ. Physical processes in the tropical tropopause layer and their roles in a changing climate". Nat Geosci 2013;6:169–76.

[5] Milz M, et al. Water vapour distributions measured with the Michelson Interferometer for Passive Atmospheric Sounding on board Envisat (MIPAS/Envisat). J Geophys Res 2005;110 D24307. doi:10.1029/2005JD005973.

[6] Stiller GP, Kiefer M, Eckert E, von Clarmann T, Kellmann S, García-Comas M, Funke B, Leblanc T, Fetzer E, Froidevaux L, Gomez M, Hall E, Hurst D, Jordan A, Kämpfer N, Lambert A, McDermid IS, McGee T, Miloshevich L, Nedoluha G, Read W, Schneider M, Schwartz M, Straub C, Toon G, Twigg LW, Walker K, Whiteman DN. Validation of MIPAS IMK/IAA temperature, water vapour, and ozone profiles with MOHAVE-2009 campaign measurements. Atmos Meas Tech 2012;5:289–320. https://doi.org/10.5194/amt-5-289-2012.

[7] Carleer MR, Boone CD, Walker KA, Bernath PF, Strong K, Sica RJ, Randall CE, Vömel H, Kar J, Höpfner M, Milz M, von Clarmann T, Kivi R, Valverde-Canossa J, Sioris CE, Izawa MRM, Dupuy E, McElroy CT, Drummond JR, Nowlan CR, Zou J, Nichitiu F, Lossow S, Urban J, Murtagh D, Dufour DG. Validation of water vapour profiles from the Atmospheric Chemistry Experiment (ACE). Atmos Chem Phys Discuss 2008;8:4499–559. doi:10.5194/acpd-8-4499-2008.

[8] Rozanov A, Weigel K, Bovensmann H, Dhomse S, Eichmann K-U, Kivi R, Rozanov V, Vömel H, Weber M, Burrows JP. Retrieval of water vapour vertical distributions in the upper troposphere and the lower stratosphere from SCIAMACHY limb measurements. Atmos Meas Tech 2011;4:933–54. https://doi.org/10.5194/amt-4-933-2011.

[9] Hurst DF, Lambert A, Read WG, Davis SM, Rosenlof KH, Hall EG, Jordan AF, Oltmans SJ. Validation of Aura Microwave Limb Sounder stratospheric water vapour measurements by the NOAA frost point hygrometer. J Geophys Res Atmos 2014;119:1612–25. doi:10.1002/2013JD020757.

[10] Riese M, Oelhaf H, Preusse P, Blank J, Ern M, FriedlVallon F, Fischer H, Guggenmoser T, Höpfner M, Hoor P, Kaufmann M, Orphal J, Plöger F, Spang R, SuminskaEbersoldt O, Ungermann J, Vogel B, Woiwode W. Gimballed limb observer for radiance imaging of the atmosphere (GLORIA) scientific objectives. Atmos Meas Tech 2014;7:1915–28. doi:10.5194/amt-7-1915-2014.

[11] Friedl-Vallon F, Gulde T, Hase F, Kleinert A, Kulessa T, Maucher G, Neubert T, Olschewski F, Piesch C, Preusse P, Rongen H, Sartorius C, Schneider H, Schönfeld A, Tan V, Bayer N, Blank J, Dapp R, Ebersoldt A, Fischer H, Graf F, Guggenmoser T, Höpfner M, Kaufmann M, Kretschmer E, Latzko T, Nordmeyer H, Oelhaf H, Orphal J, Riese M, Schardt G, Schillings J, Sha MK, Suminska-Ebersoldt O, Ungermann J. Instrument concept of the imaging Fourier transform spectrometer GLORIA. Atmos Meas Tech 2014;7:3565–77. doi:10.5194/amt-7-3565-2014.

[12] Ungermann J, Blank J, Dick M, Ebersoldt A, Friedl-Vallon F, Giez A, Guggenmoser T, Höpfner M, Jurkat T, Kaufmann M, Kaufmann S, Kleinert A, Krämer M, Latzko T, Oelhaf H, Olchewski F, Preusse P, Rolf C, Schillings J, Suminska-Ebersoldt O, Tan V, Thomas N, Voigt C, Zahn A, Zöger M, Riese M. Level 2 processing for the imaging Fourier transform spectrometer GLORIA: derivation and validation of temperature and trace gas volume mixing ratios from calibrated dynamics mode spectra. Atmos Meas Tech 2015;8:2473–89. https://doi.org/10.5194/amt-8-2473-2015.

[13] Kaufmann M, Blank J, Guggenmoser T, Ungermann J, Engel A, Ern M, Friedl-Vallon F, Gerber D, Grooß JU, Guenther G, Höpfner M, Kleinert A, Kretschmer E, Latzko Th, Maucher G, Neubert T, Nordmeyer H, Oelhaf H, Olschewski F, Orphal J, Preusse P, Schlager H, Schneider H, Schuettemeyer D, Stroh F, Suminska-Ebersoldt O, Vogel B, Volk CM, Woiwode W, Riese M. Retrieval of three-dimensional small-scale structures in upper-tropospheric/lower-stratospheric composition as measured by GLORIA. Atmos Meas Tech 2015;8:81–95. https://doi.org/10.5194/amt-8-81-2015.

[14] Montoux N, Hauchecorne A, Pommereau J-P, Lefèvre F, Durry G, Jones RL, Rozanov A, Dhomse S, Burrows JP, Morel B, Bencherif H. Evaluation of balloon and satellite water vapour measurements in the Southern tropical and subtropical UTLS during the HIBISCUS campaign. Atmos Chem Phys 2009;9:5299–319. https://doi.org/10.5194/acp-9-5299-2009.

[15] Langille JA, Solheim B, Bourassa A, Degenstein D, Brown S, Shepherd GG. Measurement of water vapour using an imaging field-widened spatial heterodyne spectrometer. Appl Opt 2017;56:4297–308.

[16] Harlander, J.M. (1991). Spatial heterodyne spectroscopy: Interferometric performance at any wavelength without scanning.

[17] Englert CR, Harlander JM, Brown CM, Marr KD. Spatial heterodyne spectroscopy at the Naval Research Laboratory. Appl Opt 2015;54:F158–63.

[18] Rodgers, Inverse methods for atmospheric sounding: theory and practice, 2000.

[19] Dupont F, Grandmont F, Solheim B, Bourassa A, degenstein D, Lloyd N, Cooney R. Spatial heterodyne spectrometer for observation of water for a balloon flight: overview of the instrument & preliminary flight data results. Fourier transform spectroscopy and hyperspectral imaging and sounding of the environment, OSA Technical Digest (online) (Optical Society of America; 2015. paper FW4A.5.

[20] Bourassa AE, Langille J, Solheim B, Degenstein D, Dupont F. The Spatial Heterodyne Observations of Water (SHOW) Instrument for high resolution profiling in the upper troposphere and lower stratosphere. Light, energy and the environ-

ment, OSA technical digest (online) (optical society of America; 2016. ,), paper FM3E.1.
[21] Dupont F, Grandmont F, Paradis S, Jacques L, Bourassa AE, Solheim B, Degenstein D, Walsh K, Kapitzke M. Spatial Heterodyne Spectrometer for Observation of Water (SHOW) aboard the ER-2 aircraft: overview of the instrument. Light, energy and the environment, OSA technical digest (online) (optical society of America; 2016. paper FM3E.2.
[22] Talbot D, et al. Development of a New Canadian operational air quality forecast model Air pollution modeling and its application XIX NATO science for peace and security Series Environmental security. Borrego C, Miranda AI, editors. Dordrecht: Springer; 2008.
[23] Bourassa AE, Degenstein DA, Llewellyn EJ. SASKTRAN: A spherical geometry radiative transfer code for efficient estimation of limb scattered sunlight. J Quant Spectrosc Radiat Transfer 2008;109(January(1)). Pages 52-73, ISSN 0022–4073. http://dx.doi.org/10.1016/j.jqsrt.2007.07.007 .
[24] Rothman LS, Gordon IE, Barbe A, Benner DC, Bernath PF, Birk M, Boudon V, Brown LR, Campargue A, Champion J-P, Chance K, Coudert LH, Dana V, Devi VM, Fally S, Flaud J-M, Gamache RR, Goldman A, Jacquemart D, Kleiner I, Lacome N, Lafferty WJ, Mandin J-Y, Massie S, Mikhailenko SN, Miller CE, Moazzen-Ahmadi N, Naumenko OV, Nikitin AV, Orphal J, Perevalov VI, Perrin A, Predoi-Cross A, Rinsland CP, Rotger M, S˘imečková M, Smith MAH, Sung K, Tashkun SA, Tennyson J, Toth RA, Vandaele AC, Auwera JV. The HITRAN 2008 molecular spectroscopic database. J Quant Spectrosc Radiat Transfer 2009;110:533–72. doi:10.1016/j.jqsrt.2009.02.013.
[25] Hedin AE. Extension of the MSIS thermosphere model into the middlelower atmosphere. J Geophys Res 1991;96:1159–72.
[26] Bourassa AE, Rieger LA, Lloyd ND, Degenstein DA. Odin-OSIRIS stratospheric aerosol data product and SAGE III intercomparison, Atmos Chem Phys, 12, 605–614, 2012. doi:10.5194/acp-12-605-2012.
[27] Zawada DJ, Dueck SR, Rieger LA, Bourassa AE, Lloyd ND, Degenstein DA. High-resolution and Monte Carlo additions to the SASKTRAN radiative transfer model. Atmos Meas Tech 2015;8:2609–23. https://doi.org/10.5194/amt-8-2609-2015.
[28] Zawada DJ, Rieger LA, Bourassa AE, Degenstein DA. Tomographic retrievals of ozone with the OMPS Limb Profiler: algorithm description and preliminary results. Atmos Meas Tech Discuss 2017. https://doi.org/10.5194/amt-2017-236 in review.
[29] Davis SP, Abrams MC, Brault JW. Introduction. Fourier transform spectrometry. San Diego: Academic Press; 2001.
[30] Englert CR, Harlander JM, Cardon JG, Roesler FL. Correction of phase distortion in spatial heterodyne spectroscopy. Appl Opt 2004;43:6680–7.
[31] Englert CR, Harlander JM. Flatfielding in spatial heterodyne spectroscopy. Appl Opt 2006;45:4583–90.
[32] Marquardt DW. An algorithm for least-squares estimation of nonlinear parameters. J Soc Indus Appl Math 1963;11(2):431–41.